ELSEVIER

Physics of the Earth and Planetary Interiors 84 (1994) 179–191

PHYSICS OF THE EARTH AND PLANETARY INTERIORS

On the measurement of anelastic attenuation using amplitudes of low-frequency surface waves

Barbara Romanowicz

Seismographic Station and Department of Geology and Geophysics, University of California, Berkeley, CA 94720, USA

(Received 9 February 1993; revision accepted 8 December 1993)

Abstract

A method is presented for the measurement of attenuation of long-period Rayleigh waves which minimizes two effects: that of biases owing to uncertainties in the source moment tensor and that of focusing owing to propagation in a laterally heterogeneous elastic Earth. In this manner, by measuring attenuation over minor arcs, odd terms of lateral heterogeneity in Q can be resolved. Global average Q estimates are in good agreement with the Preliminary Reference Earth Model (PREM) in the period range 180–285 s. At periods shorter than 180 s, our estimates of Q are lower than predicted by PREM. Maps of lateral variations in Q^{-1} show a general correspondence of high Q to high shear velocity and low Q to low shear velocity. In particular, the shift to the west, at increasing period, of the locus of the minimum in the Pacific Ocean is also observed in the Q^{-1} maps.

1. Introduction

With the availability of high-quality digital data from recently deployed global broadband networks such as GEOSCOPE and IRIS, there are now unprecedented opportunities to improve our knowledge of not only elastic, but also anelastic three-dimensional (3D) mantle structure. It is particularly important to determine the size and location of large lateral variations in Q in the upper mantle with some accuracy, and to see how they relate to lateral variations in elastic structure. Indeed, the strong dependence of Q on temperature can provide new constraints on the patterns of convection in the mantle. Also, large lateral variations in Q may cause biases, through anelastic dispersion (Liu et al., 1976), in the existing 3D elastic models. Even the latest such models (Su and Dziewonski, 1992; Woodward and Masters, 1991) have been obtained in ways that largely ignored the effects of anelasticity.

One of the advantages of the new generation of data is the possibility to measure elastic and anelastic properties of low-frequency mantle waves on the minor arc, yielding increased resolution of odd terms of structure. This was previously not possible because of limitations in the dynamic range of instruments.

A very difficult problem nevertheless inhibits the determination of accurate anelastic models from measurements of seismic amplitudes: the need to separate the effect of intrinsic attenuation from those of focusing/defocusing owing to propagation in a laterally heterogeneous elastic medium. In what follows, this problem is addressed for the case of long-period (80–300 s) fundamental mode Rayleigh waves, which can be studied in the frequency domain, using standard

SSDI 0031-9201(94)05032-S

processing techniques. A description is given of an approach that aims to minimize the effects of unknown biases both in the estimation of source amplitude and of focusing along the propagation path, and some preliminary results of the application of this approach to upper-mantle Q tomography are presented.

2. Attenuation measurements using mantle waves

To first order, the observed amplitude spectrum $A(\omega)$ of a single mode mantle Rayleigh wave is, after instrument correction, a product of three factors:

$$A(\omega) = A_s(\omega) \exp[-\eta(\omega)X] F(\omega) \quad (1)$$

where $A_s(\omega)$ is the source amplitude, $\eta(\omega)$ is the average attenuation coefficient along the path, X is the epicentral distance (in km), and $F(\omega)$ describes the focusing effects.

The source term $A_s(\omega)$ is a function of seismic moment M_o, as well as source mechanism. We here neglect effects of directivity of the source rupture. Although much progress has been achieved in recent years in the systematic estimation and reporting of seismic moments and mechanisms of large earthquakes (Dziewonski et al., 1981; Sipkin, 1982), uncertainties in seismic moment are still of the order of 30–50%, and occasionally more. To circumvent this problem, one can measure average properties over complete great circle paths (Dziewonski and Steim, 1983; Durek et al., 1993), thus eliminating the source term. Owing to symmetry properties, the sensitivity to odd terms of lateral heterogeneity is then lost, and the resulting models are incomplete: as are models based on normal mode measurements (e.g. Suda et al., 1991). Also, the frequency range of study is limited, as higher frequencies are attenuated rapidly during propagation and, for paths that have circled several times around the Earth, the signal-to-noise ratio becomes poor below periods of 130–150 s.

To resolve odd-order lateral heterogeneity (that is, heterogeneity which is not symmetrical with respect to the center of the Earth), it is necessary to incorporate measurements on single wavetrains, preferably those that correspond to low-order orbits, as they travel shorter paths and therefore contain more shorter-period energy, and more information on local structure. Single station measurements of first arriving Rayleigh wavetrains (R1 and R2) are now possible, owing to the on-scale recording of large earthquakes by modern instrumentation of the new generation global networks. Attempts at measuring lateral variations of Q at the regional level using single station measurements have been numerous (Mitchell, 1975; Canas and Mitchell, 1978; Bussy et al., 1994). However, these measurements remain sensitive to errors in the source amplitude.

One way to eliminate the source biases and retain the ability to resolve odd-order structure is to consider three consecutive wavetrains for each source–station path (Romanowicz, 1990). The following system of three equations in three unknowns is then solved for each path:

$$\log A_i(\omega) = \log A_o(\omega) - \eta_i(\omega) X_i \quad (2)$$

for $i = 1,3$, where i refers to the wavetrain R_i, and we assume that source directivity can be neglected and that attenuation is additive along the path:

$$\eta_3 X_3 = 2\eta_1 X_1 + \eta_2 X_2$$

The drawbacks of this approach are twofold. As in the case of great circle measurements, the frequency range is limited. Also, sensitivity to focusing effects is increased, especially because of the longer path travelled by the R3 wavetrain. Fig. 1 illustrates this point by showing examples of spectra of fundamental mode Rayleigh waves recorded on vertical-component instruments. The amplitude spectra of R1, R2 and R3 are compared with the theoretical source spectrum, calculated for the centroid-moment tensor (CMT) solution (Dziewonski et al., 1988). We observe the overall decrease in amplitude as a function of orbit number owing to attenuation, as expected. The smoothness of the spectrum, however, deteriorates as a function of orbit number, and is significantly poorer for R3, especially at periods shorter than 150 s, as a result of focusing effects as well as contamination from higher modes.

We are therefore faced with a trade-off: to eliminate the source, we need at least three consecutive trains; on the other hand, to make use of R3 and later arriving trains, it is necessary to take focusing effects into account, and in any case the frequency range of study is limited at the short-period end. One potentially powerful approach is to calculate the focusing effects directly, assuming that the 3D elastic model in which the waves propagate is known accurately enough, and using a theory which allows the calculation of relevant coupling effects (e.g. Lognonne, 1991; Tromp, 1992). Eventually, simultaneous inversion for elastic and anelastic structure is likely to become the appropriate approach.

Bearing in mind that currently available 3D elastic models of the upper mantle do not yet agree in their shorter-wavelength features, Romanowicz (1990) attempted to eliminate focusing effects by taking advantage of their additivity properties, which are different from those of anelastic attenuation. This involved measuring amplitudes of Rayleigh wavetrains up to R4, and solving a system of four equations for each source–station pair:

$$\log A_i(\omega) = \log A_o(\omega) - \eta_i(\omega) X_i + F_i \qquad (3)$$

for $i = 1,4$, where the number of unknowns can be reduced to four by assuming additivity of attenuation:

$$\eta_3 X_3 = 2\eta_1 X_1 + \eta_2 X_2$$
$$\eta_4 X_4 = 2\eta_2 X_2 + \eta_1 X_1 \qquad (4)$$

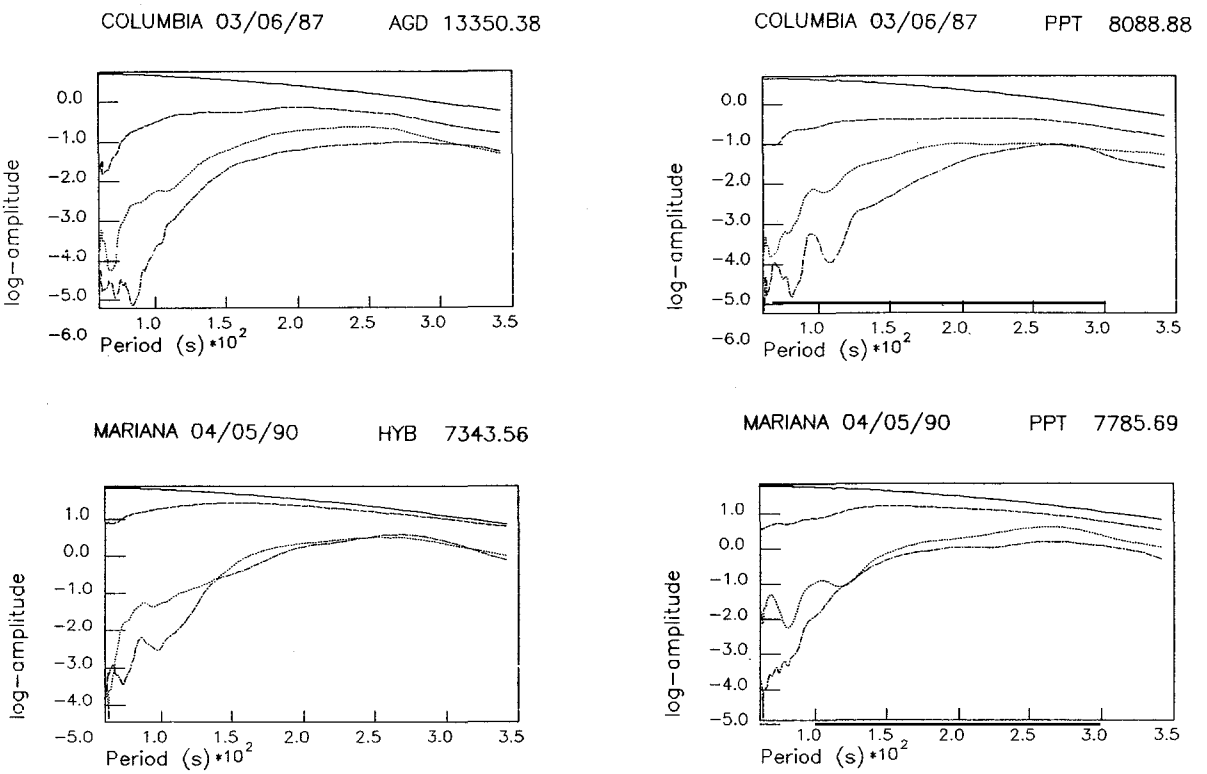

Fig. 1. Example of vertical-component Rayleigh wave amplitude spectra. The solid line is the theoretical source amplitude for the CMT solution. The broken line is for R1, the dotted line for R2 and the dashed–dotted line for R3. The logarithm of observed ampolitude is plotted after correction for instrument and geometrical spreading. For each path, epicentral distance (in km) is given after the name of the station.

and 'algebraic' additivity of focusing:

$$F_3 = 2F_1 - F_2$$

$$F_4 = 2F_2 - F_1 \quad (5)$$

This latter property arises from higher-order asymptotic calculations (Park, 1987; Romanowicz, 1987), under the strong assumption that focusing behaves in a linear fashion.

Romanowicz (1990) showed that such an approach could indeed improve the resolution of anelastic attenuation, provided the data selection was conducted very conservatively, to eliminate paths where focusing effects are stronger than allowed by the linearity assumption underlying Eqs. (5).

We here describe a 'hybrid' approach which takes into account the advantages of using first arriving trains (broader frequency range, less sensitivity to focusing) compared with those of using three consecutive wavetrains to eliminate the sensitivity to source biases. To do so, we first measure attenuation coefficients as a function of period, for each source–station pair, in two different ways: (1) assuming a known source mechanism and moment (in general, the CMT solution), and using Eq. (1) (Method 1); (2) using R_i, $i = 1,3$ and Eqns. (2) (Method 2).

We first reject those paths for which Method 1 yields attenuation coefficients that are not smooth as a function of frequency, which is indicative of contamination by focusing and other perturbing effects (e.g. higher-mode contamination at the shorter periods). Then we compare the results obtained using Methods 1 and 2. In many cases, the results agree to within 10% at the low frequencies (200–250 s), but Method 2 yields much more oscillatory results for periods shorter than 150 s. Occasionally, the two curves are shifted with respect to each other by a roughly constant amount. This is primarily due to bias in the estimate of the source moment, as well as possible errors in the instrument response function.

We have developed an interactive method which allows us to pick a suitable reference period range for the curve from Method 2 (in general around 200 s), and we shift the curve from Method 1 to make the levels of the two curves agree in that period range. This shift is modeled by a constant plus a linear trend, the latter, usually very small, accounting for errors in the source mechanism. We have tested this method

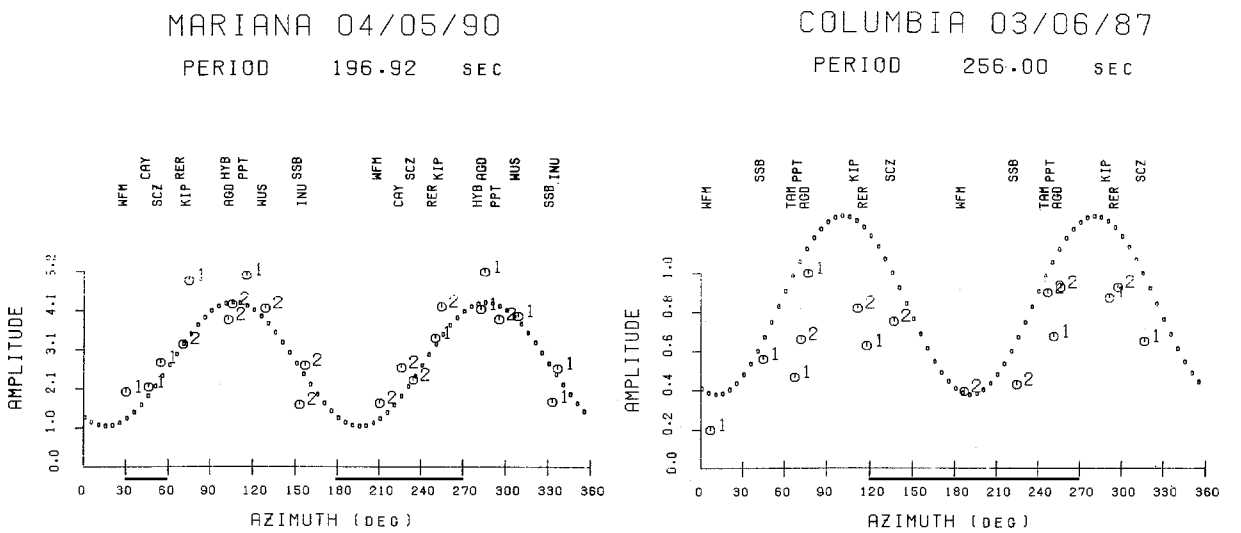

Fig. 2. Examples of amplitude radiation patterns as a function of azimuth. The dotted line is the theoretical radiation pattern for the CMT solution. ○, Data after correction for propagation using model 1066b. Numbers indicate whether the train used is R1 (1) or R2 (2). Names of stations are given above each observation point. Left: Mariana event of 5 April 1990, at a period of 197 s. Right: Colombia event of 6 March 1987, at a period of 256 s.

using synthetic data generated using normal mode summation in a spherically symmetric Earth. The tests indicate that reliable results can be obtained in the period range 100–285 s.

We note that this procedure amounts to smoothing the estimate of attenuation coefficient as a function of period obtained in Method 2, using as 'physical' constraint the shape of the curve obtained using Method 1. The source term A_0 could also be obtained, in principle, from the solution of the equations for the three consecutive trains (Method 2), but it would be more strongly contaminated by focusing and would have to be smoothed using some running average method with arbitrary choice of smoothing parameters. Also, if our assumptions are correct, we expect to obtain the same 'source shift' for R1 and R2. This is indeed the case for most of the analyzed data. We reject paths for which the difference is significant.

We also note that, although Eqns. (5) imply a linear behavior for focusing, there are strong indications that in practice focusing behaves very non-linearly. In our approach, there are no explicit restrictions on the behavior of focusing, beyond the fact that we assume that it is band-limited within the frequency band of the measurement, and not constant over this entire band.

To illustrate this procedure, we show examples for two events; the 5 April 1990 Mariana earthquake ($M_0 \approx 1.6 \times 10^{20}$ N m) and the 6 March 1987 Colombia earthquake ($M_0 \approx 0.64 \times 10^{20}$ N m) observed at stations of the GEOSCOPE network (Romanowicz et al., 1991). Fig. 2 shows the fit of the CMT solution to the observed amplitude radiation pattern at all available GEOSCOPE stations for these events, at a period of 256 s. We see that the fit is good for the Mariana event, and much poorer for the Colombia event, for which there is also much more scatter in the data.

Fig. 3 shows the minor and major arc attenuation coefficient as a function of period for several stations in the lobe of the radiation pattern, calculated using Methods 1 and 2, for the Mariana event. The theoretical curve obtained for PREM (Dziewonski and Anderson, 1981) is given for comparison. We note the agreement of the overall levels in the period range 200–250 s, and the much better-behaved character of the 'R1 only' measurement, allowing us to measure attenuation down to periods of 80–90 s for R1 and approximately 100 s for R2. A very small shift is required to bring the levels of both measurements in agreement for all stations and trains. We limit the measurement at the low-frequency end based on the level of agreement of the two determinations, and the synthetic tests. The comparison between the two measurements allows us to assess the very large size of focusing effects at some stations and in some frequency bands. For example, at KIP, in the period range 120–200 s and for R1, the hole in the spectrum observed in Fig. 1 is reflected in an effect which is twice as large as the theoretical value for model 1066b (Gilbert and Dziewonski, 1975), although the departure from model 1066b using R1 is, in this case, only a few per cent. It should be noted that this hole in the spectrum cannot be accounted for by higher-mode contamination, as synthetic tests indicate. Also, a simple smoothing procedure, such as running average, applied to the curve obtained using Method 2 would have led to biased results at periods shorter than 200 s. These examples also show that it is generally impossible to use Method 2 for periods shorter than 130 s.

Fig. 4 shows corresponding examples for the 1987 Colombia event. In this case, in addition to much smoother results using Method 1, we note a large shift between the curves from Methods 1 and 2. This shift is consistent between R1 and R2 for a given station, as well as from one station to the other (it is of the order of -0.3), indicating that it is mostly due to bias in the seismic moment of the earthquake, which is overestimated by about 30%. This is in agreement with the difference in moment reported in the National Earthquake Information Center (NEIC) bulletin for the CMT (0.64×10^{20} N m) and a body-wave moment tensor solution (0.35×10^{20} N m). Our measurement indicates a moment of approximately 0.4×10^{20} N m. The differences between the final determination (R1 only, after shifting) and PREM are several times smaller than what they would be if the theoretical source amplitude was taken at face value. The residual differences,

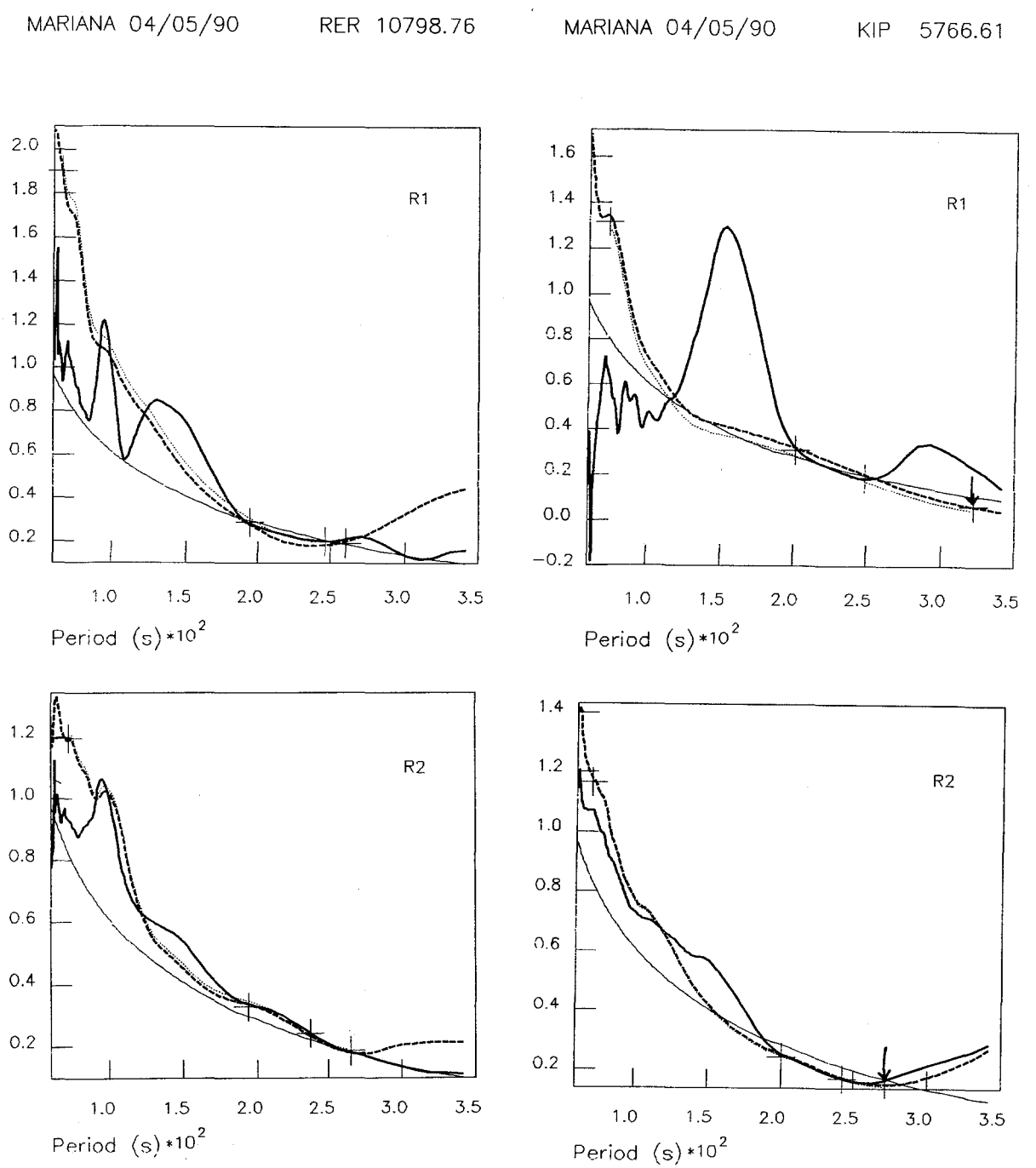

Fig. 3. Examples of attenuation coefficient determination for the 5 April 1990 Mariana event at GEOSCOPE Stations RER (left) and KIP (right). Epicentral distance (in km) is given after the name of the station. (Attenuation coefficients are in $km^{-1} \times 10^4$.) Thin solid line: reference model 1066b. Thick solid line: determination using R1, R2 and R3 (Method 2). Thick broken line: determination using only R1 (Method 1). Dotted line: final determination using R1 after shifting the broken line curve to match the thick solid line in the period range indicated by crosses. Arrows indicate the period range in which the final data are kept for future inversion.

in the period range where the curve from Method 2 is 'well-behaved', between the two determinations after the shift has been applied, give us a measure of the uncertainty in the measurement of attenuation coefficient, which is here of the order of 10–15%.

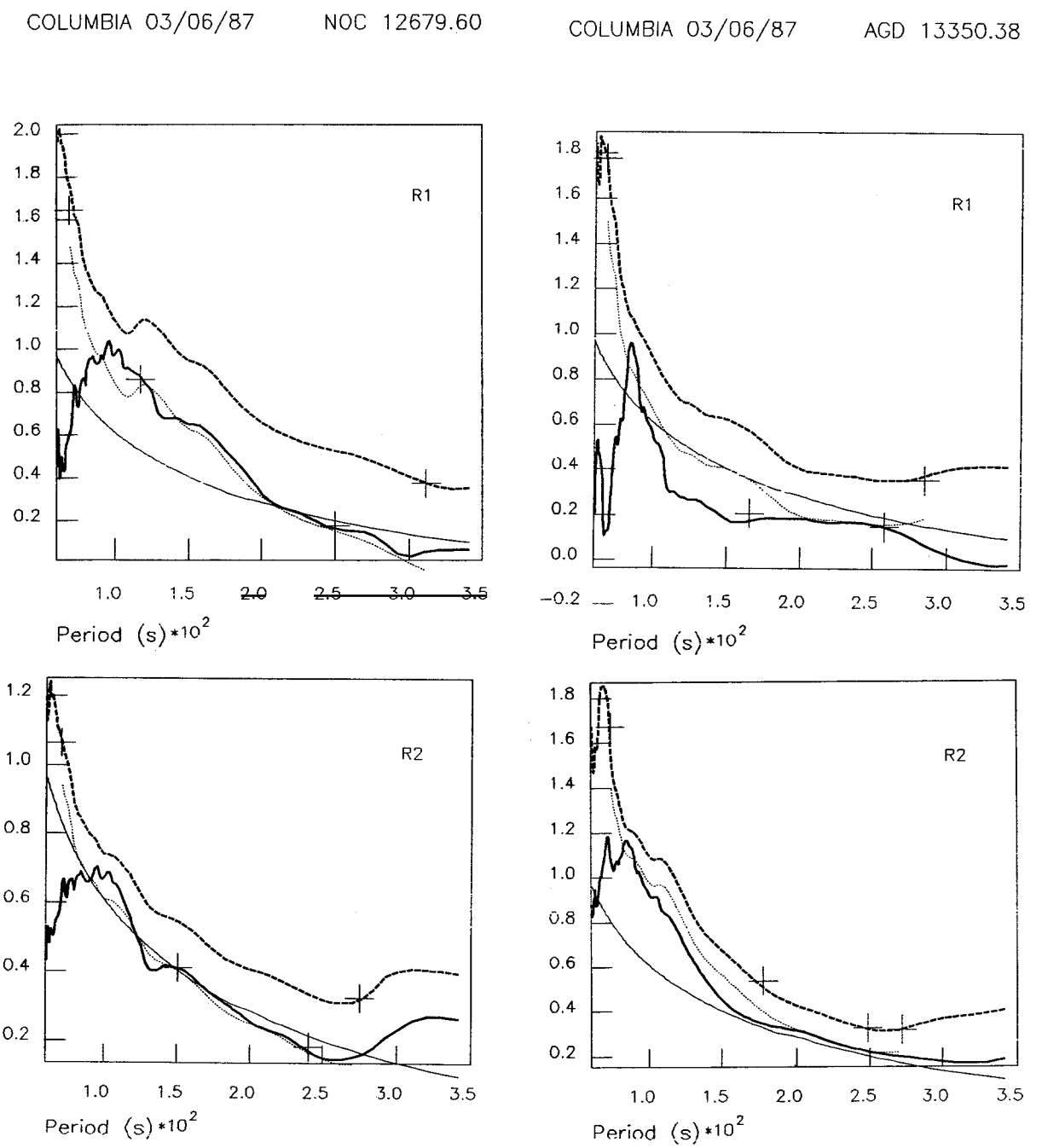

Fig. 4. Same as Fig. 3 for the Colombia event of 6 March 1987, observed at GEOSCOPE Stations NOC (left) and AGD (right).

In summary, our approach allows us to reduce considerably the uncertainty in the measurement of attenuation coefficients along minor and major arcs by: (1) selecting paths and period ranges for which the R1-only and R2-only measurements are minimally affected by focusing; (2) correcting for biases in the source amplitude when necessary; (3) extending the period range of measurement to below 100 s.

The examples shown indicate that errors as large as 50–100% can be introduced if precautions equivalent to those described here are not applied. Although iterative simultaneous inversion for elastic and anelastic structure as well as source parameters should, in the future, allow much less time-consuming, automatized algorithms to be used in attenuation tomography, we feel that, at present, the careful inspection of data involved in our procedure is necessary.

3. Estimation of global average Q and departure from spherical symmetry

Many workers have published estimates of global averages of Q in the upper mantle, using various datasets and measurement techniques. A debate has recently been opened (Durek, 1993) as to which of these measurements represent the 'true' average global Q. Indeed, results fall into two subsets. The first subset includes studies based on normal mode amplitude measurements (Deschamps, 1977; Sailor and Dziewonski, 1978; Jobert and Roult, 1978) and studies based on measurements of mantle wave amplitudes (Dziewonski and Steim, 1983; Romanowicz, 1990; Durek et al., 1993). These measurements agree, within their standard deviations, with PREM (Dziewonski and Anderson, 1981), at least in the period range 140–250 s. The second subset comprises results of measurements of complex amplitudes of normal modes (Masters and Gilbert, 1983; Smith and Masters, 1989; Widmer et al., 1991), which consistently yield higher Q values at periods greater than 180 s.

The reason for these differences is as yet unknown and is the subject of current investigations. It could either be a bias caused by sampling of the globe (the latter group has averaged measurements over more paths than the former), or one owing to the influence of elastic structure, which could affect the amplitude measurements differently from those of complex eigenfrequencies.

In Table 1 and Fig. 5, we present our measurements of global average Q and compare them with PREM and values of Widmer et al. (1991). Our dataset originally consists of 722 single train measurements (R1 and R2) using the method described in this paper. Records used are for large earthquakes ($M_s > 6.7$) in the 5 year period 1987–1992 observed at stations of the GEOSCOPE and IRIS–IDA networks. After visual inspection of amplitude plots (e.g. Fig. 3), we reject paths for which the final attenuation coefficient is not smooth as a function of frequency, or for which the source level cannot be determined accurately through a comparison of Methods 1 and 2. We also reject outliers by imposing the constraint that relative departure from the mean should not exceed 50% for R1 and 30% for R2.

Table 1
Comparison of measurements of $Q^{-1} \times 10^3$ obtained in this study with PREM (Dziewonski and Anderson, 1981) and measurements reported by Widmer et al. (1991) ('QM1')

Period (s)	y_1	σ_1	N_1	y_2	σ_2	N_2	PREM	QM1
284.44	5.26	1.1	265	5.23	0.87	61	5.09	4.34
269.47	5.34	1.0	332	5.37	0.6	63	5.34	4.50
256.00	5.45	1.0	354	5.52	0.6	64	5.57	4.95
232.73	5.95	1.1	371	5.99	0.7	64	5.98	5.37
213.33	6.48	1.2	378	6.52	0.7	65	6.32	5.64
200.78	6.80	1.2	373	6.84	0.7	65	6.55	6.00
182.86	7.28	1.2	376	7.32	0.8	65	6.90	6.55
170.67	7.67	1.3	365	7.68	1.0	65	7.13	6.83
160.00	7.98	1.4	352	8.07	1.1	65	7.36	6.80
150.59	8.25	1.4	328	8.21	1.0	65	7.56	
140.27	8.57	1.5	300	8.48	1.0	65	7.8	
128.00	8.87	1.5	281	8.77	1.0	64	8.06	
120.47	8.96	1.5	269	8.95	0.9	65	8.18	
110.11	9.15	1.4	258	9.20	0.8	63	8.33	
100.39	9.30	1.4	245	9.34	0.9	62	8.4	

y_i, σ_i and N_i are respectively estimates of standard deviation and number or measurements used in the calculation; $i = 1$ corresponds to a straight average of the data; $i = 2$ is a weighted average, according to a scheme described in the text; N_2 represents the number of cells hit by the data.

This reduces the dataset to some 350 measurements.

To minimize biases caused by uneven sampling of the globe, we attach weights to the data, inversely proportional to the number of samples in the bin they belong to. The binning is done in the following way. We divide the Earth's surface into 30° by 30° cells and assign each path to the cell which contains the pole position for the great circle joining epicenter and station. The pole position is the positive pole (in a counter-clockwise convention) if the longitude of the mid-point on the path is in one meridian hemisphere, and it is the negative pole otherwise. This allows us to distinguish contributions from minor and major arcs. We note that 65 out of 72 cells have been hit at least once in the binning process.

The global average values of $(1/Q) \times 1000$ obtained in this fashion are given in Table 1 and compared with averages obtained without binning. The differences are small, indicating that spatial biasing is most probably not an issue. The average values are in better agreement with PREM than with the measurements of Widmer et al. The agreement with PREM is excellent between 180–285 s. At shorter periods, our results indicate a lower on average Q than predicted by PREM, although the latter does lie within the error bars of our measurements. However, PREM was constructed from a dataset which did not include any fundamental mode constraints at periods shorter than 150 s.

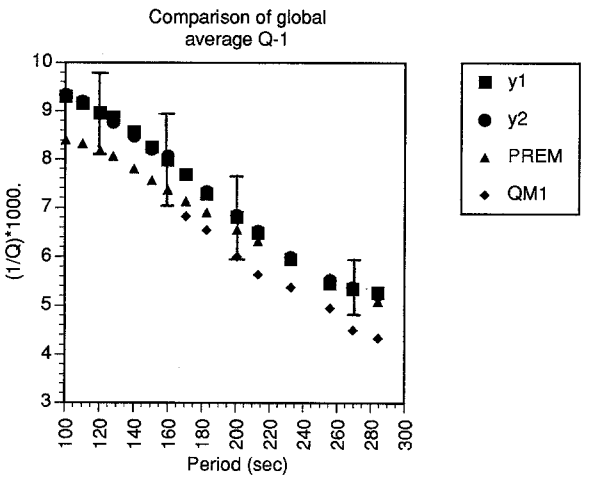

Fig. 5. Comparison of global average Q^{-1} measurements. Averages for this study are y_1 (unweighted average) and y_2 (weighted average) and are compared with PREM (Dziewonski and Anderson, 1981) and the values reported by Widmer et al. (1991) (QM1). Error bars correspond to the y_2 measurement.

In our global average measurements, the standard deviations are large. Our 3D modeling shows that a large proportion of the variance in the data can be explained by simple models of lateral heterogeneity in Q. There is now abundant evidence from surface-waves and free oscillations for the existence of large lateral variations in upper-mantle Q, reaching in excess of 50% (Nakanishi, 1978; Roult, 1982; Dziewonski and Steim, 1983; Romanowicz, 1990). To illustrate this, Fig. 6 gives an example of two paths sampling different geographical regions, for which we have four independent measurements of attenuation coefficient, using the method described in this paper, allowing us to estimate an upper bound on standard deviations in the measurements. For each example presented, the four events were located within 500 km of each other.

The R1 path from the Solomon Islands to Station KIP in Hawaii is entirely within the Pacific Ocean, and the measurement reflects the high attenuation in this area across the entire frequency band. On the other hand, R2 averages over a longer distance, and the values obtained are close to PREM except below a period of 120 s.

The R1 path from the Philippines to TAM in Algeria is a continental path sampling in particular the 'cold' western Pacific subduction zone area. The attenuation coefficient for this path is small at periods longer than 150 s. For R2, the path samples parts of the Pacific and Atlantic Oceans, and the resulting average attenuation coefficient is high at periods shorter than 200 s.

These two examples confirm the existence of strong lateral variations in Q in the upper mantle, which can reach in excess of $\pm 50\%$ and contribute to the standard deviation in the global average Q. The bias to lower Q values as compared with the Widmer et al. measurements cannot be explained by a straightforward effect of sampling. It is probably related to the interaction

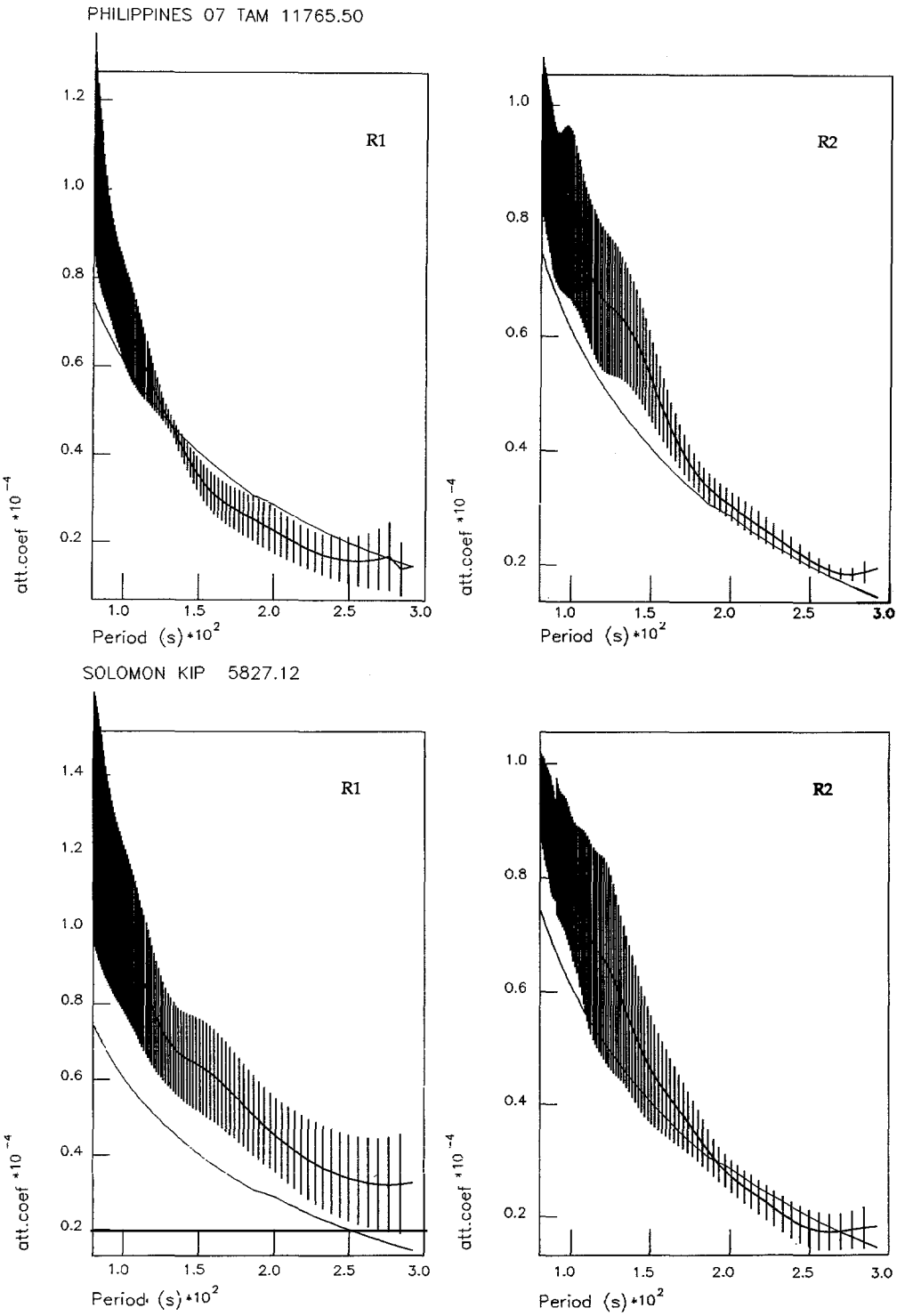

Fig. 6. Examples of average attenuation coefficients and corresponding standard deviations for two paths for which four earthquakes were available within 500 km of each other. The thin solid line is the reference 1066b model. The average epicentral distance is indicated after the name of the station.

of lateral heterogeneity in the elastic and anelastic parts of the Earth that are taken into account differently according to the method used. Comparisons of single record measurements are now being conducted, to clarify this point.

4. Examples of maps of lateral variations in Q^{-1}

We present in Fig. 7 some examples of maps of lateral variations in Q^{-1} obtained using the dataset and the method described in this paper. Complete 3D models will be presented elsewhere. These maps were obtained using an inversion method with no a priori basis functions (Tarantola and Valette, 1982) as adapted to the case of surface waves by Montagner (1986). The spatial wavelength resolution corresponds to a spherical harmonics expansion up to approximately order six. The maps shown in Fig. 7 confirm our previous results (Romanowicz, 1990) and show that, in general, oceanic regions are characterized by high attenuation whereas stable regions and subduction zones have low attenuation. At shorter periods (e.g. 128 s), the high-attenuation regions are concentrated around mid-ocean ridges, especially in the Pacific, but also in the Atlantic and Indian Oceans. At progressively

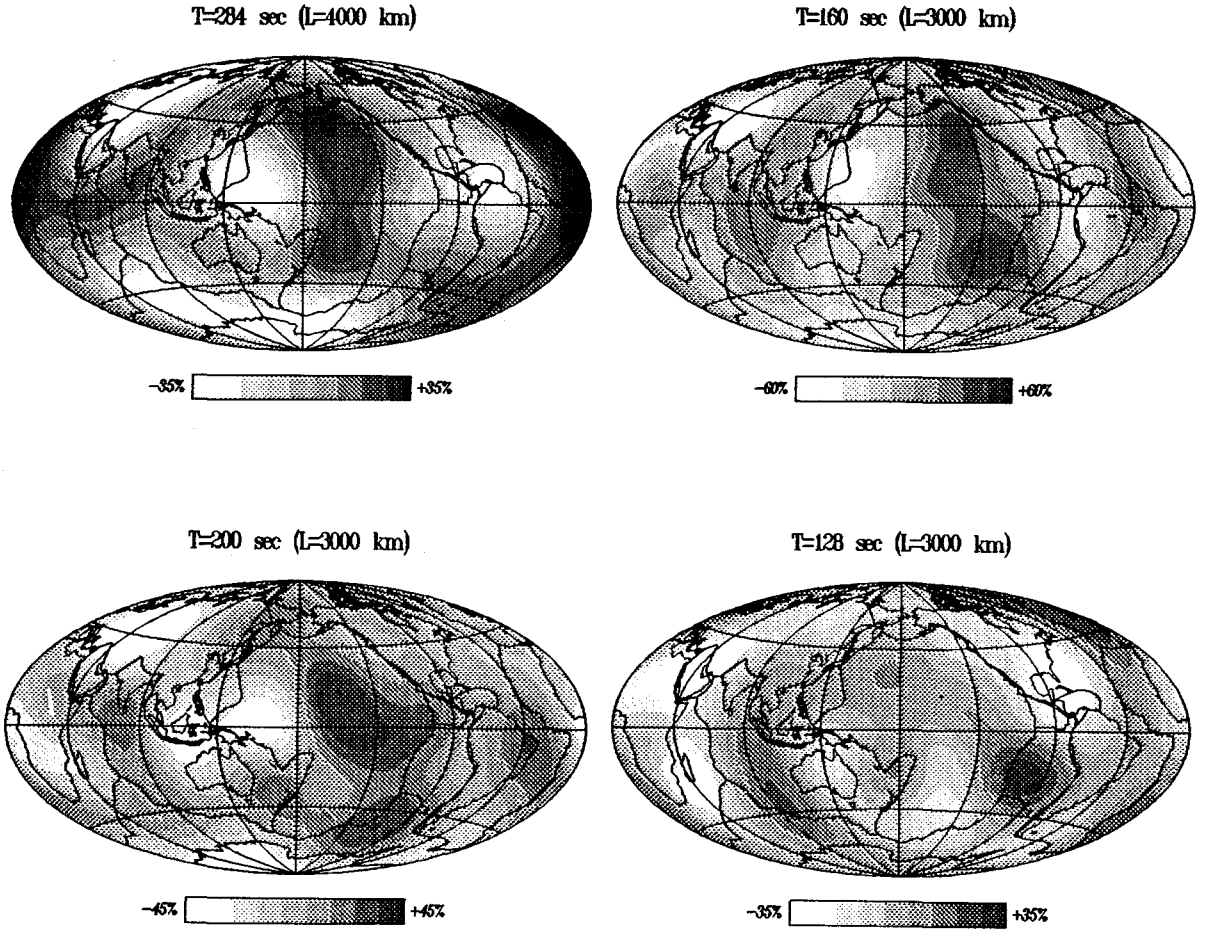

Fig. 7. Examples of maps of lateral variations in $Q^{-1} \times 10^3$, with respect to the mean at each period. The correlation length is $L = 3000km$ at all periods except at 284 s where it is 4000 km. Variance reduction is 46% at 284 s, 60% at 200 s, 55% at 160 s and 42% at 128 s. Final errors in the maps are very uniform and of the order of 15%.

longer periods, in the Pacific Ocean, the high-attenuation zone is shifted from the East Pacific Rise towards the central Pacific. Such a shift is also observed in a recent regional study (Bussy et al., 1994) as well as in elastic models (e.g. Montagner and Tanimoto, 1991; Su and Dziewonski, 1992). The largest lateral variations seem to occur in the period range 150–200 s, but persist at longer periods, indicating that large lateral variations in Q persist throughout the upper mantle.

5. Discussion and conclusions

We have presented a method of measurement of mantle wave attenuation which allows us to retrieve information on the odd part of lateral heterogeneity in the upper mantle Q. This method requires careful inspection of the data, and many observations need to be rejected because they are strongly contaminated by focusing effects. Sampling tests indicate that this does not significantly affect the resulting global average $Q(\omega)$, which is closer to PREM than to recent results of Widmer et al. (1991), but in agreement with other studies (Durek and Ekstrom, 1992). Maps of lateral variations of Q^{-1} at various periods obtained using this new procedure confirm earlier results and indicate a general correspondence of regions of high velocity to regions of high Q and regions of low velocity to regions of low Q. The low values of Q which we obtain at periods shorter than 180 s are in agreement with results of regional studies.

We believe that our procedure yields results that are relatively free of contamination by focusing because it involves measurements on short travelled trains and a comparison between two estimations, following which many measurements are rejected. It relies, however, on the assumption that focusing effects are band limited within the frequency band of interest, that is, they do not mimic a quasi-constant source bias over the entire band. This assumption needs to be further investigated by studying the non-linear effects of lateral heterogeneity on amplitudes, which are not accessible using first-order asymptotic theory.

Acknowledgments

This work was supported through NSF Grants EAR-9104674 and EAR-9204631. David Sharrock participated in the development of the interactive graphic software used in this study.

References

Bussy, M., Montagner, J.P. and Romanowicz, B., 1994. Tomographic study of upper mantle attenuation in the Pacific Ocean. Geophys. Res. Lett., 20: 663–666.

Canas, J.A. and Mitchell, B.J., 1978. Lateral variation of surface-wave anelastic attenuation across the Pacific. Bull. Seismol. Soc. Am., 68: 1637–1650.

Deschamps, A., 1977. Inversion of the attenuation data of free oscillations of the Earth (fundamental and first higher modes). Geophys. J.R. Astron. Soc., 50: 699–722.

Durek, J. and Ekstrom, G., 1992. Differences between observations of fundamental mode attenuation. EOS Trans. Am. Geophys. Union, 73: 402.

Durek, J., Ritzwoller, M. and Woodhouse, J:H., 1993. Constraining upper mantle anelasticity using surface wave amplitude anomalies. Geophys. J. Int., 114: 249–272.

Dziewonski, A.M. and Anderson, D.L., 1981. Preliminary Reference Earth Model. Phys. Earth Planet. Inter., 25: 297–356.

Dziewonski, A.M. and Steim, J., 1983. Dispersion and attenuation of mantle waves through waveform inversion. Geophys. J.R. Astron. Soc., 70: 503–527.

Dziewonski, A.M., Chou, G. and Woodhouse, J.H., 1981. Determination of earthquake source parameters from waveform modelling. J. Geophys. Res., 86: 2825–2852.

Dziewonski, A.M., Ekstrom, G., Woodhouse, J. and Zwart, G., 1988. Centroid-moment tensor solutions for January–March, 1987. Phys. Earth Planet. Inter., 50: 116–126.

Gilbert, F. and Dziewonski, A.M., 1975. An application of normal mode theory to the retrieval of structural parameters and source mechanism from seismic spectra. Philos. Trans. R. Soc. London, Ser. A, 278: 187–269.

Jobert, N. and Roult, G., 1978. Periods and damping of free oscillations observed in France after sixteen earthquakes. Geophys. J.R. Astron. Soc., 45: 155–176.

Liu, H.P., Anderson, D.L. and Kanamori, H., 1976. Velocity dispersion due to anelasticity; implication for seismology and mantle composition. Geophys. J.R. Astron. Soc., 47: 41–58.

Lognonne, Ph., 1991. Normal modes and seismograms in an anelastic rotating earth. J. Geophys. Res., 96: 20309–20319.

Masters, G. and Gilbert, F., 1983. Attenuation in the earth at low frequencies. Philos. Trans. R. Soc. London, 308: 479–522.

Mitchell, B.J., 1975. Regional Rayleigh wave attenuation in North America. J. Geophys. Res., 80: 4904–4916.

Montagner, J.P., 1986. Regional three-dimensional structures using long-period surface waves. Ann. Geophys. 4B3: 283–294.

Montagner, J.P. and Tanimoto, T., 1991. Global anisotropy in the upper mantle inferred from the regionalisation of phase velocities. J. Geophys. Res., 95: 4797–4819.

Nakanishi, I., 1978. Regional differences in the phase velocity and the quality factor Q of mantle Rayleigh waves. Science, 200: 1379–1381.

Park, J., 1987. Asymptotic coupled mode expressions for multiplet amplitude anomalies and frequency shifts on an aspherical earth. Geophys. J.R. Astron. Soc., 90: 129–164.

Romanowicz, B., 1987. Multiplet–multiplet coupling due to lateral hetergeneity asymptotic effects on the amplitude and frequency of the Earth's normal modes, Geophys. J.R. Astron. Soc., 90: 75–100.

Romanowicz, B., 1990. The upper mantle degree 2: constraints and inferences from global mantle wave attenuation measurements. J. Geophys. Res., 95: 11051–11071.

Romanowicz, B., Karczewski, J.F., Cara, M., Bernard, P., Borsenberger, J., Cantin, J.M., Dole, B., Fouassier, D., Koenig, J.C., Morand, M., Pillet, R., Pyrolley, A. and Rouland, D., 1991. The Geoscope Program: present status and perspectives. Bull. Seism. Soc. Am., 81: 243–264.

Roult, G., 1982. The effect of young oceanic regions on frequencies and damping of free oscillations of the Earth. J. Geophys., 51: 38–43.

Sailor, R.V. and Dziewonski, A.M., 1978. Measurements and interpretation of normal mode attenuation. Geophys. J.R. Astron. Soc., 53: 559–581.

Sipkin, R., 1982. Estimation of earthquake source parameters by the inversion of waveform data: synthetic seismograms. Phys. Earth Planet. Inter., 30: 242–259.

Smith, M.F. and Masters, G., 1989. Aspherical structure constraints from free oscillation frequency and attenuation measurements. J. Geophys. Res., 94: 1953–1976.

Su, W. and Dziewonski, A., 1992. On the scale of mantle heterogeneity. Phys. Earth Planet. Inter., 74: 29–54.

Suda, N., Shibata, N. and Fukao, Y., 1991. Degree-2 pattern of attenuation structure in the upper mantle from apparent complex frequency measurements of fundamental spheroidal modes. Geophys. Res. Lett., 18: 1119–1122.

Tarantola, A. and Valette, B., 1982. Generalized nonlinear inverse problems solved using the least squares criterion. Rev. Geophys., 20: 219–232.

Tromp, J., 1992. Inversion of surface wave phase and amplitude anomalies. EOS Trans. Am. Geophys. Union, 73: 396.

Widmer, R., Masters, G. and Gilbert, F., 1991. Spherically symmetric attenuation within the earth from normal mode data. Geophys. J. Int., 104: 541–553.

Woodward, R. and Masters, G., 1992. Upper mantle structure from long-period differential travel times and free oscillation data. Geophys. J. Int., 109: 275–293.